Journal of Catalysis **193,** 65–79 (2000)
doi:10.1006/jcat.2000.2878, available online at http://www.idealibrary.com on IDEAL®

$YBa_2Cu_3O_{7-\delta}X_\sigma$ (X = F and Cl): Highly Active and Durable Catalysts for the Selective Oxidation of Ethane to Ethene

H. X. Dai, C. F. Ng, and C. T. Au[1]

Department of Chemistry and Center for Surface Analysis and Research, Hong Kong Baptist University, Kowloon Tong, Hong Kong, China

Received October 21, 1999; accepted March 24, 2000

The catalytic performance and characterization of $YBa_2Cu_3O_{7-\delta}$ and $YBa_2Cu_3O_{7-\delta}X_\sigma$ for the oxidative dehydrogenation of ethane (ODE) to ethene have been investigated. Under the reaction conditions of temperature = 680°C, $C_2H_6/O_2/N_2$ molar ratio = 2/1/3.7, and contact time = 1.67×10^{-4} h g ml^{-1}, $YBa_2Cu_3O_{7-0.21}F_{0.16}$ showed 84.1% C_2H_6 conversion, 81.8% C_2H_4 selectivity, and 68.8% C_2H_4 yield; $YBa_2Cu_3O_{7-0.18}Cl_{0.13}$ showed 92.5% C_2H_6 conversion, 72.0% C_2H_4 selectivity, and 66.6% C_2H_4 yield. The sustainable performance during a period of 40 h on-stream reaction at 680°C demonstrated that the F- and Cl-doped catalysts are durable. X-ray powder diffraction results indicated that the undoped $YBa_2Cu_3O_{7-\delta}$ and halide-doped $YBa_2Cu_3O_{7-\delta}X_\sigma$ were of triple-layered oxygen-deficient perovskite-type orthorhombic structure. The results of the X-ray photoelectron spectroscopy, thermal treatment, thermogravimetric analysis, and $^{18}O_2$-pulsing studies indicated that the incorporation of halide ions into the $YBa_2Cu_3O_{7-\delta}$ lattice enhanced the activity of lattice oxygen. According to the O_2 temperature-programmed desorption and temperature-programmed reduction results, we conclude that the oxygen species desorbed at 610–710°C are active for the selective oxidation of ethane and those desorbed below 610°C are active for the total oxidation of ethane; a suitable oxygen nonstoichiometry and Cu^{3+} concentration in $YBa_2Cu_3O_{7-\delta}X_\sigma$ are required for the best catalytic performance of the catalysts.

Key Words: **ethane selective oxidation; ethene generation; oxidative dehydrogenation; ODE reaction; superconducting material; perovskite-type oxide catalyst; halide-incorporated $YBa_2Cu_3O_{7-\delta}$.**

INTRODUCTION

In the past decades, the oxidative dehydrogenation of ethane (ODE) to ethene has been investigated extensively and intensively. Many materials have been used as catalysts for this reaction. Among them, the Li^+-MgO-Cl^--based catalyst (1) seems to be the most effective: 75% C_2H_6 conversion, 77% C_2H_4 selectivity, and ca. 58% C_2H_4 yield under the reaction conditions of temperature = 620°C, C_2H_6/O_2/He molar ratio = 1/1/0.62, and contact time = 1.39×10^{-3} h g ml^{-1}. Although $KSr_2Bi_3O_4Cl_6$ (2), a layered complex compound, gave a C_2H_4 yield of ca. 70% at 640°C, the catalyst deteriorated due to Cl leaching. In recent years, many researchers have reported that perovskite-type oxides such as $SrCo_{0.8}Li_{0.2}O_3$ (3), $SrCo_{0.8}Fe_{0.2}O_3$ and $La_{0.8}Sr_{0.2}CoO_3$ (4), $CaCo_{0.8}Fe_{0.2}O_3$ (5), and $La_{0.6}Sr_{0.4}Co_{0.8}Fe_{0.2}O_3$ (6) showed moderate catalytic performance for the OCM (oxidative coupling of methane) reaction. More recently, after investigating a series of $La_{1-x}Sr_xFeO_{3-\delta}$ catalysts, Yi *et al.* (7) reported a C_2H_6 conversion of 87% and a C_2H_4 selectivity of 43% and a corresponding C_2H_4 yield of 37% over a $SrFeO_{3-\delta}$ catalyst under the reaction conditions: temperature = 650°C, C_2H_6/O_2 molar ratio = 1/1, and contact time = 1.43×10^{-4} h g ml^{-1}.

Perovskite materials are known to be active for the total oxidation of carbon monoxide and hydrocarbons (8, 9). The oxygen vacancies and strong redox ability of these compounds play important roles in the catalysis of a complete oxidation reaction. Generally speaking, the higher the oxygen vacancy density and the stronger the redox ability, the better is the performance of the perovskite-type oxide catalyst. Since the discovery of high-T_c superconductor $YBa_2Cu_3O_{7-\delta}$ (10–13), many researchers employed such a material as catalyst for chemical reactions. For example, Hansen *et al.* reported that for the oxidation and ammoxidation of toluene to generate benzaldehyde and benzonitrile, respectively, the selectivity and activity observed over $YBa_2Cu_3O_{6+x}$ were better than those observed over other oxides such as V_2O_5 (14). Mizuno *et al.* observed an uptake of NO and CO in large quantities by $YBa_2Cu_3O_{6+x}$ and believed that the formation of CO_2 and N_2 was due to the interaction of adsorbed CO and NO (15). The good catalytic performance of $YBa_2Cu_3O_{7-\delta}$ for CO oxidation was related to the amount of oxygen sites and electrical conductivity of the catalyst (16). After the synthesis of the fluorinated superconducting $YBa_2Cu_3O_yF_2$ material (with a T_c as high as 155 K) by Ovshinsky *et al.* (17), Lee and Ng used $YBa_2Cu_2O_{6+x-z}F_z$ compounds as catalysts for the partial oxidation of methane and found that the incorporation of F^- ions enhanced the tendency for the partial oxidation reaction (18). $YBa_2Cu_3O_{7-\delta}$ is of triple-layered

[1] To whom correspondence should be addressed. E-mail: pctau@hkbu.edu.hk.

0021-9517/00 $35.00

perovskite structure and is known to have a high density of oxygen vacancies and show strong redox ability. If one could decrease the oxygen vacancy density (thus reducing complete oxidation) and increase the redox ability (thus strengthening selective oxidation) by incorporating F^- or Cl^- ions (which have ionic radii similar to that of O^{2-} ion) to the oxygen vacancies, one would convert these combustion materials to catalysts which are selective for the oxidation of ethane to ethene. Based on this idea, we generated several classes of halide-doped perovskite-type oxide catalysts. In our previous studies, we characterized $SrFeO_{3-\delta}Cl_\sigma$ (19) and $La_{1-x}Sr_xFeO_{3-\delta}X_\sigma$ ($x =$ 0–0.8, $X =$ F and Cl) (20) catalysts which showed good activity and durability for the ODE reaction. In this study, we examined the catalytic performance of perovskite-type halo-oxide $YBa_2Cu_3O_{7-\delta}X_\sigma$ ($X =$ F and Cl) as well as $YBa_2Cu_3O_{7-\delta}$ (for comparison purposes) and characterized them by using X-ray diffraction (XRD), X-ray photoelectron spectroscopy (XPS), thermogravimetric analysis (TGA), O_2 temperature-programmed desorption (O_2-TPD), temperature-programmed reduction (TPR), and pulsing techniques.

EXPERIMENTAL

The catalysts were prepared from the appropriate amounts of (i) $Y(NO_3)_3 \cdot 6H_2O$, $Ba(NO_3)_2$, $Cu(NO_3)_2 \cdot 3H_2O$ for $YBa_2Cu_3O_{7-\delta}$, (ii) $Y(NO_3)_3 \cdot 6H_2O$, $Ba(NO_3)_2$, $Cu(NO_3)_2 \cdot 3H_2O$, and CuF_2 for $YBa_2Cu_3O_{7-\delta}F_\sigma$, and (iii) $Y(NO_3)_3 \cdot 6H_2O$, $Ba(NO_3)_2$, $Cu(NO_3)_2 \cdot 3H_2O$, and $CuCl_2 \cdot 2H_2O$ for $YBa_2Cu_3O_{7-\delta}Cl_\sigma$. In order to control the amount of F^- ions in $YBa_2Cu_3O_{7-\delta}$, CuF_2 was employed as a precursor (21) and added according to the amount of F^- required for $YBa_2Cu_3O_{7-\delta}F_\sigma$ generation, the remaining amount of copper required was added in the form of $Cu(NO_3)_2 \cdot 3H_2O$. The same method was used for the preparation of $YBa_2Cu_3O_{7-\delta}Cl_\sigma$. After dissolving these powders in deionized water and mixing with citric acid equimolar to the metals, the solution was kept at 75°C for water evaporation until the solution became viscous. The mixture was then heated at 85°C for 6 h to produce an amorphous material which was then heated in air at 960°C for 12 h. The calcined substance was ground and pressed into disk-shaped pellets. The pellets were sintered at 960°C in air for 12 h and then slowly cooled to room temperature, followed by crushing and sieving into a size range of 80–100 mesh.

The activity measurement was performed at atmospheric pressure with 0.5 g of the catalyst and 5.0 g quartz sand being placed in a fixed-bed quartz microreactor (i.d. = 4 mm). The flow rate was 14.8 ml min^{-1} for ethane and 35.2 ml min^{-1} for air, giving a contact time of 1.67×10^{-4} h g ml^{-1} and a $C_2H_6/O_2/N_2$ molar ratio of 2/1/3.7. The product mixture (C_2H_6, C_2H_4, CH_4, CO, and CO_2) was determined on line by gas chromatograph (Shimadzu 8A TCD) with Porapak Q and 5A Molecular Sieve being the columns. For the variation of contact time, the reactant flow rate was changed at a fixed catalyst mass (0.5 g). The balances of carbon and oxygen were estimated to be 100 ± 2 and $100 \pm 3\%$, respectively, for every run over the catalysts.

The crystal structures of the catalysts were determined by an X-ray diffractometer (D-MAX, Rigaku) operating at 40 kV and 200 mA using Cu$K\alpha$ radiation. The patterns recorded were referred to the powder diffraction files—PDF-2 Database for the identification of crystal phases. X-ray photoelectron spectroscopy (XPS, Leybold Heraeus-Shenyang SKL-12) was used to determine the O 1*s* and Cu 2*p* binding energies of surface oxygen and copper species. Before XPS measurements, the samples were calcined in O_2 (flow rate, 20 ml min^{-1}) at 800°C for 1 h and then cooled in O_2 to room temperature, followed by thermal treatments in He (20 ml min^{-1}) at the desired temperatures for 1 h and then cooling in He to room temperature. The treated samples were then outgassed in the primary vacuum chamber (10^{-5} torr) for 0.5 h and then introduced into the ultrahigh vacuum chamber (3×10^{-9} torr) for recording. The C 1*s* line at 284.6 eV was taken as a reference for binding energy calibration. The specific surface areas of the catalysts were measured using a Nova 1200 apparatus.

The TGA experiments were carried out on a thermal analyzer (Shimadzu DT-40) containing an electrobalance. The sample (20 mg) was kept in a flow of nitrogen (20 ml min^{-1}) and heated from room temperature to 800°C at a rate of 20°C min^{-1}. Before performing the TGA experiment, the sample was in turn treated in a He flow of 20 ml min^{-1} at 800°C for 1 h, evacuated *in situ* at the same temperature for 1 h, purged with O_2 (20 ml min^{-1}) for 1 h, and cooled in O_2 to room temperature. Such a treatment was to guarantee the complete removal of adsorbed CO_2 and H_2O from the sample.

We performed pulse experiments to investigate the reactivity of surface oxygen species. A catalyst sample (0.2 g) was placed in a microreactor and was thermally treated at a desired temperature for 30 min before the pulsing of C_2H_6 or C_2H_6/O_2 (2/1 molar ratio) and the effluent was analyzed online by a mass spectrometer (HP G1800A). In order to confirm the involvement of surface lattice oxygen in the ODE reaction, we treated the sample at a desired temperature in He (flow rate, 20 ml min^{-1}) for 1 h and then kept on pulsing $^{18}O_2$ at a lower temperature until no observable change of pulse size was detected. After purging with He for 0.5 h, we pulsed C_2H_6 or CO onto the treated sample and analyzed the effluent compositions. The pulse size was 65.7 μl (at 25°C, 1 atm) and He (HKO Co., purity >99.995%) was the carrier gas.

The procedures of O_2-TPD and TPR experiments as well as halogen content analysis in the catalysts were as those described previously (20, 22).

The oxidation states of copper ions in the superconducting catalysts were determined using a popular titrimetric analysis method based on the oxidation of ferrous ion (23–26)

$$Cu^{3+} + Fe^{2+} \rightarrow Cu^{2+} + Fe^{3+}, \quad [1]$$

or the reduction of ferric ion (24)

$$Cu^{+} + Fe^{3+} \rightarrow Cu^{2+} + Fe^{2+}. \quad [2]$$

The sample (ca. 0.2 g) was dissolved in 2.6 M H_3PO_4 solution containing standard 0.1 M Fe^{2+} (Mohr's salt, $(NH_4)_2Fe(SO_4)_2 \cdot 6H_2O$) solution under an inert (N_2) atmosphere. The Fe^{2+} that remained after the above reaction was titrated with standard 0.017 M potassium dichromate. As for the determination of Cu^+ content, the sample (ca. 0.2 g) was dissolved in 2.6 M H_3PO_4 solution containing standard 0.1 M Fe^{3+}; Fe^{3+} was reduced to Fe^{2+} via reaction step [2] and the Fe^{3+} ions could be determined by titrating the solution against standardized 0.017 M potassium dichromate solution (24). The indicator was sodium 4-diphenylamine sulfonate. The experimental error for the determination of Cu^{3+} content is estimated to be ±0.10%.

RESULTS

Catalyst Composition and Crystal Structure

Table 1 shows the crystal structures, compositions, and surface areas of $YBa_2Cu_3O_{7-\delta}$ and $YBa_2Cu_3O_{7-\delta}X_\sigma$. According to the PDF-2 data (No. 39-486), we deduce that these three catalysts are of orthorhombic structure. The results of Cu^+ titration analysis indicated the absence of Cu^+ ions in these catalysts. According to the contents of halogen, Cu^{3+} and Cu^{2+} as well as assuming electroneutrality, the δ value was estimated to be 0.28 for $YBa_2Cu_3O_{7-\delta}$; for the five $YBa_2Cu_3O_{7-\delta}F_\sigma$ catalysts studied, the δ and σ values were 0.27 and 0.10, 0.24 and 0.13, 0.21 and 0.16, 0.18 and 0.19, 0.18 and 0.22, respectively. As for $YBa_2Cu_3O_{7-\delta}Cl_\sigma$, the δ and σ values were 0.18 and 0.13. The incorporation of F^- and Cl^- ions in the $YBa_2Cu_3O_{7-\delta}$ lattice did not induce any significant decrease in surface area. After 40 h of on-stream reaction, there was little change in F or Cl content. From Table 1, one can also observe that the inclusion of halide ions in $YBa_2Cu_3O_{7-\delta}$ caused the Cu^{3+} content to increase and the nonstoichiometric oxygen, i.e., oxygen vacancy density, to decrease.

Catalytic Performance

In a blank experiment, 5.0 g of quartz sand gave a C_2H_6 conversion of 7.6%, a C_2H_4 selectivity of 89.2%, and a C_2H_4 yield of 6.8% at 680°C. It indicates that quartz sand is poor in catalytic activity. Figure 1 shows the catalytic performance of $YBa_2Cu_3O_{7-0.28}$, $YBa_2Cu_3O_{7-\delta}F_\sigma$, and $YBa_2Cu_3O_{7-0.18}Cl_{0.13}$. Over the $YBa_2Cu_3O_{7-0.28}$ catalyst (Fig. 1(I)), with the rise in temperature from 500 to 680°C, C_2H_6 conversion, C_2H_4 selectivity, and C_2H_4 yield increased from 18.2, 12.2, and 2.2% to 45.4, 42.7, and 19.4%, respectively; CO_x selectivity decreased from 87.8 to 55.5%; O_2 conversion reached 100% at 640°C; CH_4 selectivities were less than 2% within the temperature range studied. Over $YBa_2Cu_3O_{7-\delta}F_\sigma$ (Figs. 1(IIa–e)), with the increase in temperature, C_2H_6 and O_2 conversions, CH_4 selectivity, and C_2H_4 yield increased; C_2H_4 selectivity reached a maximum value at 660°C, whereas CO_x selectivity came to a minimum value. Table 2 shows the performance of the $YBa_2Cu_3O_{7-\delta}F_\sigma$ catalysts at 660°C. Among the five F-doped catalysts, $YBa_2Cu_3O_{7-0.21}F_{0.16}$ showed the best performance; at 660°C, C_2H_6 conversion, C_2H_4 selectivity, and C_2H_4 yield were 82.2, 82.3, and 67.7%, respectively. Over the $YBa_2Cu_3O_{7-0.18}F_{0.13}$ catalyst (Fig. 1(III)), with the rise in temperature from 500 to 680°C, C_2H_6 and O_2 conversions, C_2H_4 yield, and CH_4 selectivity augmented from 7.7, 28.1, 4.0, and 0%, respectively, to 92.5, 96.8, 66.6, and 5.5%; C_2H_4 selectivity reached a maximum value of 73.8% at 660°C; CO_x selectivity decreased from 47.8 to 22.5%; at 680°C, C_2H_4 yield reached a maximum value of 66.6%. Compared to the undoped catalyst, the halide-doped catalysts showed much higher C_2H_4 selectivities at lower C_2H_6 conversion (<ca. 30%) levels (Figs. 1(I, IIc, and III)).

TABLE 1

Crystal Structures, Compositions, and Surface Areas of $YBa_2Cu_3O_{7-\delta}$ and $YBa_2Cu_3O_{7-\delta}X_\sigma$ Catalysts

Catalyst	Crystal phase	X Content (wt%)	Cu^{3+} (mol%)	Cu^{2+} (mol%)	δ	σ	Nonstoichiometric oxygen (mol)	Surface area ($m^2\ g^{-1}$)
$YBa_2Cu_3O_{7-\delta}$	Orthorhombic	—	23.9	76.1	0.28	—	0.28	1.62
$YBa_2Cu_3O_{7-\delta}F_\sigma$	Orthorhombic	0.29	24.4	75.6	0.27	0.10	0.17	1.60
	Orthorhombic	0.37	25.2	74.8	0.24	0.13	0.11	1.58
	Orthorhombic	0.46(0.45)[a]	26.4	73.6	0.21	0.16	0.05	1.57
	Orthorhombic	0.54	27.4	72.6	0.18	0.19	0	1.56
	Orthorhombic	0.63	28.6	71.4	0.18	0.22	0	1.54
$YBa_2Cu_3O_{7-\delta}Cl_\sigma$	Orthorhombic	0.69(0.67)[a]	27.2	72.8	0.18	0.13	0.05	1.59

[a] After 40 h of on-stream ODE reaction.

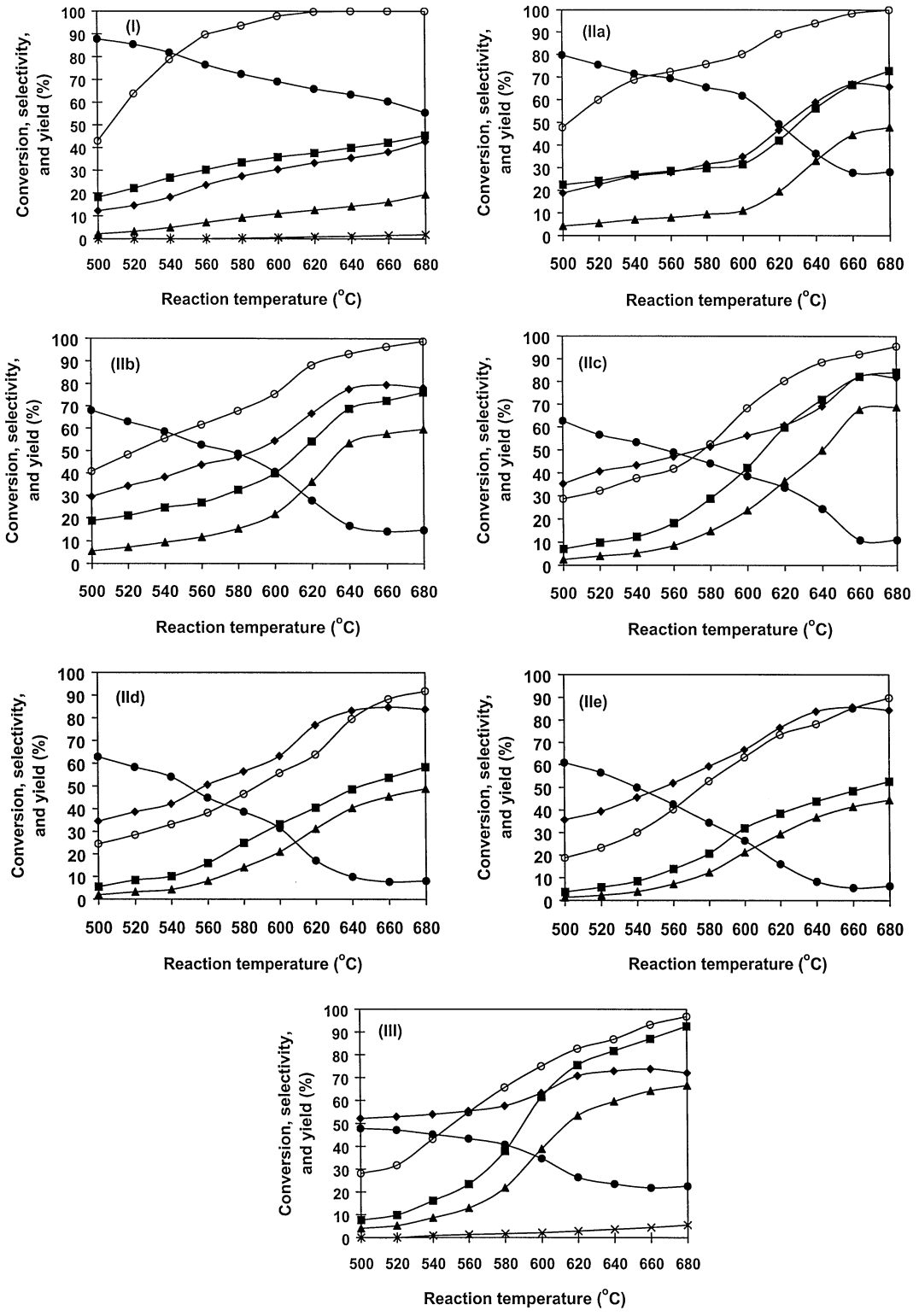

FIG. 1. Catalytic performance of (I) $YBa_2Cu_3O_{7-0.28}$, (IIa) $YBa_2Cu_3O_{7-0.27}F_{0.10}$, (IIb) $YBa_2Cu_3O_{7-0.24}F_{0.13}$, (IIc) $YBa_2Cu_3O_{7-0.21}F_{0.16}$, (IId) $YBa_2Cu_3O_{7-0.18}F_{0.19}$, (IIe) $YBa_2Cu_3O_{7-0.18}F_{0.22}$, and (III) $YBa_2Cu_3O_{7-0.18}Cl_{0.13}$ as related to reaction temperature. (■) C_2H_6 conversion, (◆) C_2H_4 selectivity, (▲) C_2H_4 yield, (○) O_2 conversion, (●) CO_x ($CO + CO_2$) selectivity, and (X) CH_4 selectivity.

TABLE 2

Catalytic Performance of the $YBa_2Cu_3O_{7-\delta}F_\sigma$ Catalysts at 660°C and 1.67 × 10^{-4} h g ml^{-1}

Catalyst	Conversion (%)		Selectivity (%)	Yield (%)	Rate of C_2H_6 reaction
	C_2H_6	O_2	C_2H_4	C_2H_4	(10^{19} molecules m^{-2} s^{-1})
$YBa_2Cu_3O_{7-0.27}F_{0.10}$	66.5	98.4	66.8	44.4	0.081
$YBa_2Cu_3O_{7-0.24}F_{0.13}$	72.4	96.4	79.5	57.6	0.089
$YBa_2Cu_3O_{7-0.21}F_{0.16}$	82.2	92.1	82.3	67.7	0.102
$YBa_2Cu_3O_{7-0.18}F_{0.19}$	53.7	88.2	84.7	45.5	0.067
$YBa_2Cu_3O_{7-0.18}F_{0.22}$	48.4	85.2	85.7	41.5	0.061

Figure 2 shows the catalytic performance of $YBa_2Cu_3O_{7-0.21}F_{0.16}$ and $YBa_2Cu_3O_{7-0.18}Cl_{0.13}$ at 680°C as a function of on-stream reaction time. It is apparent that the performances of the two catalysts were rather stable. In other words, they were durable within a period of 40 h.

The catalytic performance of $YBa_2Cu_3O_{7-0.21}F_{0.16}$ and $YBa_2Cu_3O_{7-0.18}Cl_{0.13}$ as related to contact time at 680°C is shown in Fig. 3. With the rise in contact time from 0.63×10^{-4} to 2.50×10^{-4} h g ml^{-1} over the F-doped catalyst (Fig. 3a), C_2H_6 and O_2 conversions and CO_x selectivity increased from 51.7, 70.7, and 5.8% to 87.8, 98.8, and 16.4%, respectively; C_2H_4 selectivity decreased from 87.2 to 75.9%, whereas C_2H_4 yield reached a maximum value of 68.8% at a contact time of 1.67×10^{-4} h g ml^{-1}. Over the Cl-doped catalyst (Fig. 3b), C_2H_6 and O_2 conversions and CO_x selectivity increased from 61.6, 73.4, and 14.3% to 94.4, 98.2, and 24.8%, respectively; C_2H_4 selectivity decreased from 80.2 to 70.1% whereas C_2H_4 yield reached a maximum value of 67.6% at a contact time of 1.25×10^{-4} h g ml^{-1}. Similar results were obtained when the two catalysts were well dispersed in quartz sand.

XPS, TGA, C_2H_6-, and C_2H_6/O_2-Pulsing Studies

The XPS spectra of Cu 2*p* for $YBa_2Cu_3O_{7-0.28}$, $YBa_2Cu_3O_{7-0.21}F_{0.16}$, and $YBa_2Cu_3O_{7-0.18}Cl_{0.13}$ exhibited

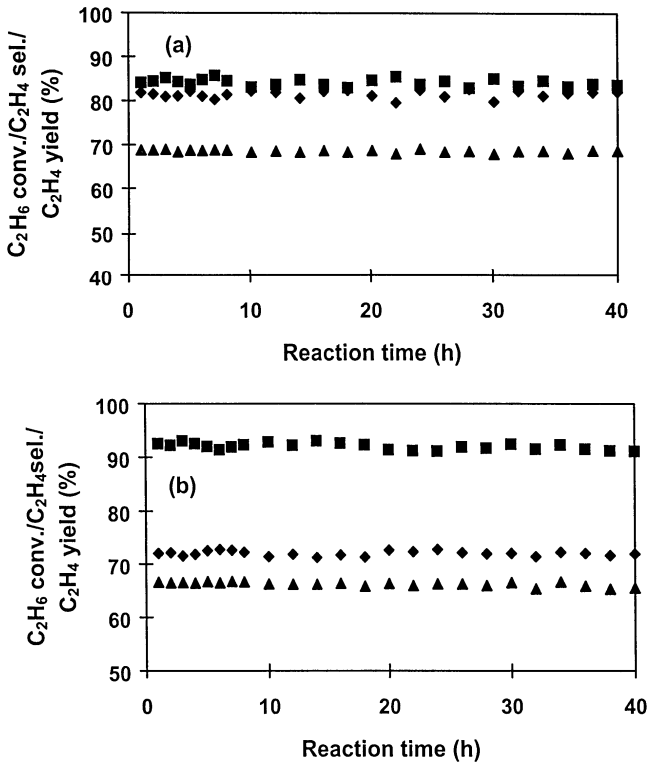

FIG. 2. Catalytic performance of (a) $YBa_2Cu_3O_{7-0.21}F_{0.16}$ and (b) $YBa_2Cu_3O_{7-0.18}Cl_{0.13}$ as a function of reaction time at 680°C. (■) C_2H_6 conversion, (◆) C_2H_4 selectivity, and (▲) C_2H_4 yield.

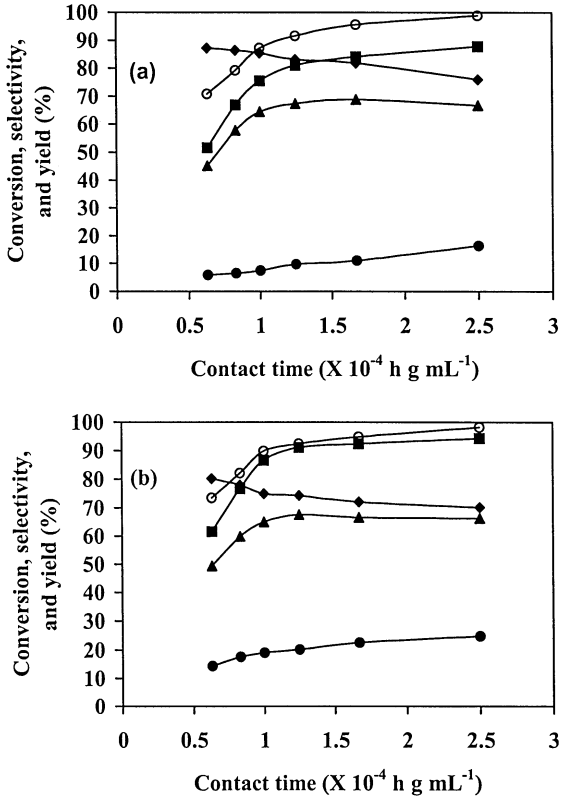

FIG. 3. Catalytic performance of (a) $YBa_2Cu_3O_{7-0.21}F_{0.16}$ and (b) $YBa_2Cu_3O_{7-0.18}Cl_{0.13}$ as related to contact time at 680°C. (■) C_2H_6 conversion, (◆) C_2H_4 selectivity, (▲) C_2H_4 yield, (○) O_2 conversion, and (●) CO_x selectivity.

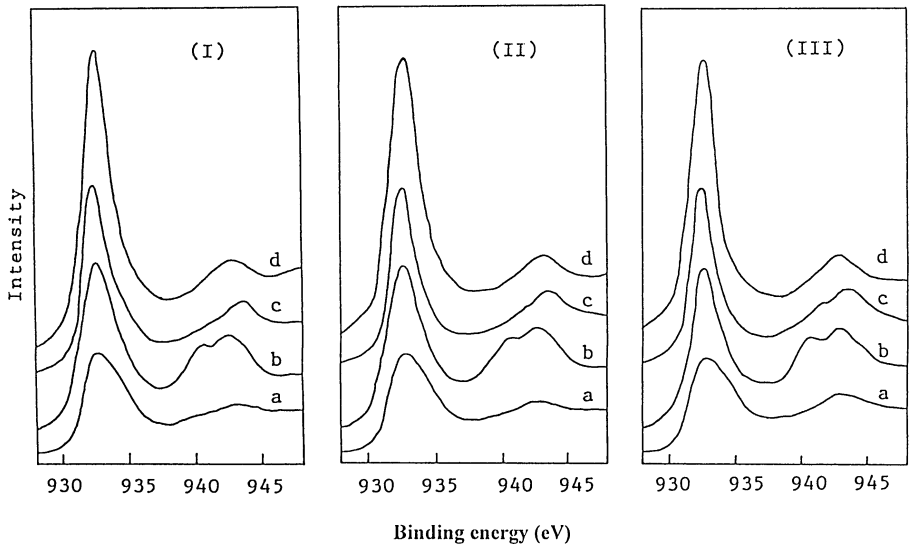

FIG. 4. Cu $2p_{3/2}$ XPS spectra of (I) $YBa_2Cu_3O_{7-0.28}$, (II) $YBa_2Cu_3O_{7-0.21}F_{0.16}$, and (III) $YBa_2Cu_3O_{7-0.18}Cl_{0.13}$ after treatment in air (a) at 25°C, (b) at 480°C for $YBa_2Cu_3O_{7-0.28}$, 510°C for $YBa_2Cu_3O_{7-0.21}F_{0.16}$, and 500°C for $YBa_2Cu_3O_{7-0.18}Cl_{0.13}$, (c) at 610°C, and (d) 710°C.

two main peaks corresponding to the $2p_{1/2}$ and $2p_{3/2}$ levels and shake-up satellites were observed about 10 eV from the main peaks. Figure 4 shows the Cu $2p_{3/2}$ spectra of the samples that had been heated at various temperatures. One can observe that the feature of the shake-up satellite became the most apparent at a heating temperature of 480°C for $YBa_2Cu_3O_{7-0.28}$, 510°C for $YBa_2Cu_3O_{7-0.21}F_{0.16}$, and 500°C for $YBa_2Cu_3O_{7-0.18}Cl_{0.13}$. Among the three catalysts, with the rise in temperature, the satellite signal intensity decreased in the order of $YBa_2Cu_3O_{7-0.21}F_{0.16} > YBa_2Cu_3O_{7-0.18}Cl_{0.13} \gg YBa_2Cu_3O_{7-0.28}$; the Cu $2p_{3/2}$ binding energy increased in the sequence of $YBa_2Cu_3O_{7-0.21}F_{0.16} < YBa_2Cu_3O_{7-0.18}F_{0.13} < YBa_2Cu_3O_{7-0.28}$.

The O 1*s* XPS spectra of $YBa_2Cu_3O_{7-0.28}$, $YBa_2Cu_3O_{7-0.21}F_{0.16}$, and $YBa_2Cu_3O_{7-0.18}Cl_{0.13}$ after being heated at various temperatures are shown in Fig. 5. For $YBa_2Cu_3O_{7-0.28}$ (Fig. 5(I)), the O 1*s* spectrum at 25°C exhibited three components *r*, *s*, and *t*, at binding energies 533.0, 531.2, and 528.4 eV, corresponding to dioxygen or carbonate, monoxygen, and lattice oxygen species (27). The intensity ratio of these three peaks was estimated to be ca. 1/2/1. Apparently, such an intensity ratio and the peak positions of the three components changed with the rise in treatment temperature. The intensities of *r* and *s* decreased whereas the intensity of *t* increased. The *r* component disappeared at 500°C and above 610°C, the

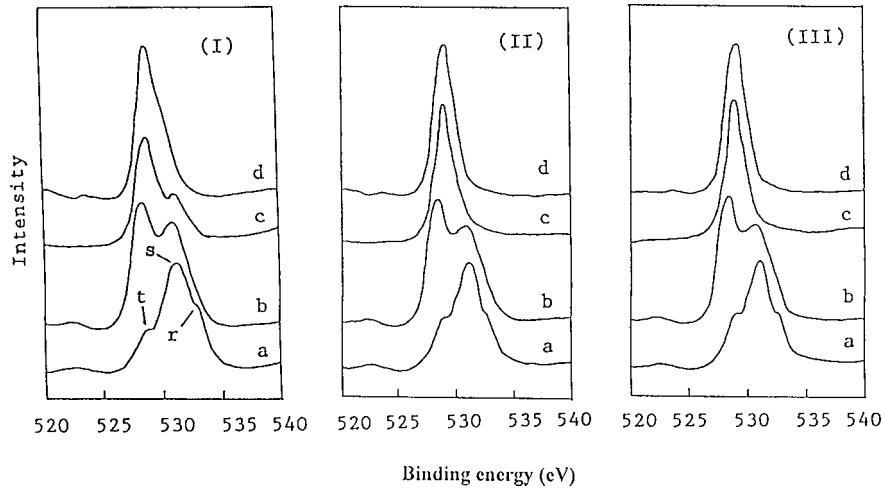

FIG. 5. O 1*s* XPS spectra of (I) $YBa_2Cu_3O_{7-0.28}$, (II) $YBa_2Cu_3O_{7-0.21}F_{0.16}$, and (III) $YBa_2Cu_3O_{7-0.18}Cl_{0.13}$ after treatment in air: (a) at 25°C, (b) at 480°C for $YBa_2Cu_3O_{7-0.28}$, 510°C for $YBa_2Cu_3O_{7-0.21}F_{0.16}$, and 500°C for $YBa_2Cu_3O_{7-0.18}Cl_{0.13}$, (c) at 610°C, and (d) at 710°C.

TABLE 3

TGA Results of $YBa_2Cu_3O_{7-\delta}$ and $YBa_2Cu_3O_{7-\delta}X_\sigma$ Catalysts

Catalyst	Weight loss (wt%)		Weight loss (wt%)[a]	
	<610°C	610–800°C	<610°C	610–800°C
$YBa_2Cu_3O_{7-0.28}$	0.74	0.19	0.68	0.54
$YBa_2Cu_3O_{7-0.27}F_{0.10}$	0.44	0.36	0.41	0.56
$YBa_2Cu_3O_{7-0.24}F_{0.13}$	0.30	0.44	0.27	0.63
$YBa_2Cu_3O_{7-0.21}F_{0.16}$	0.15	0.56	0.12	0.70
$YBa_2Cu_3O_{7-0.18}F_{0.19}$	0.07	0.63	0	0.76
$YBa_2Cu_3O_{7-0.18}F_{0.22}$	0.03	0.68	0	0.77
$YBa_2Cu_3O_{7-0.18}Cl_{0.13}$	0.14	0.53	0.12	0.77

[a] Calculations based on the desorption of the oxygen adsorbed at oxygen vacancies below 610°C ($2Cu^{3+} + 2O^-_{vacancy} \rightarrow 2Cu^{2+} + O_2$) and the desorption due to partial Cu^{3+} reduction between 610 and 800°C ($2Cu^{3+} + O^{2-}_{lattice} \rightarrow 2Cu^{2+} + 1/2O_2$).

intensity of the *t* component became larger than that of the *s* component. With the rise in treatment temperature, the position of *s* shifted to higher binding energy. For the F- and Cl-doped catalysts (Figs. 5(II, III)), the peak at ca. 533.2 eV binding energy decreased in intensity with the rise in treatment temperature and disappeared completely at and above 710°C, whereas the peaks at ca. 529.4 eV for the F-doped sample and at ca. 529.1 eV for the Cl-doped sample intensified and shifted to higher binding energies. The corresponding O 1*s* binding energy of $YBa_2Cu_3O_{7-0.21}F_{0.16}$ (ca. 530.1 eV) was slightly higher than that of $YBa_2Cu_3O_{7-0.18}Cl_{0.13}$ (ca. 529.7 eV) at 710°C.

The TGA results obtained over $YBa_2Cu_3O_{7-0.28}$ and $YBa_2Cu_3O_{7-\delta}X_\sigma$ are listed in Table 3. There were weight losses below 610°C and between 610 and 710°C. The weight loss below 610°C was due to the desorption of oxygen located at oxygen vacancies and that between 610 and 710°C due to the reduction of a certain amount of Cu^{3+} to Cu^{2+}. Compared to the theoretically calculated values, the weight losses below 610°C were rather similar whereas those between 610 and 710°C were less. Below 610°C, $YBa_2Cu_3O_{7-0.28}$ showed the largest weight loss (0.65%), whereas between 610 and 710°C, the undoped catalyst showed a loss much smaller than the theoretical value of partial Cu^{3+} reduction. With the rise in F content in the F-doped catalysts, the weight loss below 610°C decreased but that between 610 and 710°C increased.

Table 4 shows the changes of Cu^{3+} contents in $YBa_2Cu_3O_{7-0.28}$, $YBa_2Cu_3O_{7-0.21}F_{0.16}$, and $YBa_2Cu_3O_{7-0.18}Cl_{0.13}$ after the samples were heated in He at various temperatures. With the increase in treatment temperature from 610 to 710°C, there was significant decrease in the Cu^{3+} content. The exposure of the thermally treated samples to an oxygen flow at the same temperature would result in the restoration of the Cu^{3+} contents. The weight losses calculated according to the changes in Cu^{3+} ion contents are rather close to those observed between 610 and 710°C in the TGA experiments. Furthermore, after heat treatment at 710°C, the halide content in each of the three catalysts was rather similar to that of the fresh catalyst. It indicates that there was no significant halogen leaching during the course of calcination at 710°C.

Table 5 shows the C_2H_6 conversions and C_2H_4 selectivities observed when the thermally treated $YBa_2Cu_3O_{7-0.28}$, $YBa_2Cu_3O_{7-0.21}F_{0.16}$, and $YBa_2Cu_3O_{7-0.18}Cl_{0.13}$ samples were exposed, respectively, to C_2H_6 or C_2H_6/O_2 (molar ratio = 2/1) pulses at a temperature similar to that of thermal treatment. In the case of pulsing C_2H_6, with the rise in treatment temperature from 500 to 710°C, C_2H_6 conversions and C_2H_4 selectivities increased significantly over the three catalysts; at 710°C, the C_2H_6 conversion and C_2H_4 selectivity were, respectively, 56.2 and 63.1% over $YBa_2Cu_3O_{7-0.28}$, 86.4 and 79.1% over $YBa_2Cu_3O_{7-0.21}F_{0.16}$, and 94.2 and 74.6% over $YBa_2Cu_3O_{7-0.18}Cl_{0.13}$. If the

TABLE 4

The Changes of Cu^{3+} Contents in $YBa_2Cu_3O_{7-0.28}$, $YBa_2Cu_3O_{7-0.21}F_{0.16}$, and $YBa_2Cu_3O_{7-0.18}Cl_{0.13}$ after Thermal Treatments in He at Temperatures Corresponding to the Oxygen Desorptions Illustrated in Fig. 6

Catalyst	Cu^{3+} Content (mol%)		Halide content (wt%)[a]	Weight loss (wt%)[b]	
	610°C	710°C	710°C	<610°C	610–710°C
$YBa_2Cu_3O_{7-0.28}$	14.7 (23.8)[c]	9.2 (23.5)	—	0.66	0.20
$YBa_2Cu_3O_{7-0.21}F_{0.16}$	24.9 (29.0)	9.1 (28.7)	0.44	0.11	0.57
$YBa_2Cu_3O_{7-0.18}Cl_{0.13}$	25.1 (28.9)	10.1 (28.8)	0.68	0.10	0.56

[a] Halide contents of the samples thermally treated in He at 710°C for 0.5 h.

[b] Weight losses were estimated based on the changes in Cu^{3+} content.

[c] Values in parentheses were obtained after the thermally treated sample was exposed to an oxygen flow 20 ml min^{-1} at the same temperature for 0.5 h.

TABLE 5

Catalytic Performance of $YBa_2Cu_3O_{7-0.28}$, $YBa_2Cu_3O_{7-0.21}F_{0.16}$, and $YBa_2Cu_3O_{7-0.18}Cl_{0.13}$ in a C_2H_6 or C_2H_6/O_2 Pulse after Being Thermally Treated in He, Respectively, at 500, 610, and 710°C for 0.5 h

	500°C [a]		610°C [a]		710°C [a]	
Catalyst	C_2H_6 Conv. (%)	C_2H_4 Sel. (%)	C_2H_6 Conv. (%)	C_2H_4 Sel. (%)	C_2H_6 Conv. (%)	C_2H_4 Sel. (%)
$YBa_2Cu_3O_{7-0.28}$	17.4 [b]	14.1	30.4	36.7	56.2	63.1
	(18.9) [c]	(15.6)	(34.6)	(32.8)	(54.7)	(46.8)
$YBa_2Cu_3O_{7-0.21}F_{0.16}$	5.6	18.8	62.6	75.1	86.4	79.1
	(7.9)	(22.7)	(66.3)	(75.6)	(87.1)	(80.6)
$YBa_2Cu_3O_{7-0.18}Cl_{0.13}$	6.4	20.9	63.4	66.2	94.2	74.6
	(8.8)	(25.6)	(65.8)	(67.4)	(89.6)	(68.2)

[a] Temperature for thermal treatment and reactant pulsing.
[b] In a pulse of C_2H_6.
[c] Values in parentheses were obtained in a pulse of C_2H_6/O_2 (molar ratio = 2/1).

thermal treatment temperatures were at or below 710°C, the behaviors of C_2H_6 conversions and C_2H_4 selectivities in the C_2H_6- and C_2H_6/O_2-pulsing experiments were rather similar.

$^{18}O_2$ Isotope, Ethane, and Carbon Monoxide Pulsing Studies

We conducted $^{18}O_2$, C_2H_6, and CO pulsing experiments over $YBa_2Cu_3O_{7-0.21}F_{0.16}$ and $YBa_2Cu_3O_{7-0.18}Cl_{0.13}$ which had been treated under a number of conditions. In the case of pulsing C_2H_6 over the $^{18}O_2$-treated catalysts, besides C_2H_6, C_2H_4, and their fragments, we detected three signals with $m/e = 20$, 19, and 18, corresponding to $H_2{}^{18}O$, ^{18}OH, and ^{18}O, respectively, indicating that surface lattice oxygen ^{18}O (incorporated in the $YBa_2Cu_3O_{7-\delta}X_\sigma$ lattice during $^{18}O_2$-pulsing) had reacted with C_2H_6. In the case of CO pulsing, besides CO and its fragments, we detected a signal with $m/e = 46$, corresponding to $CO^{18}O$; the results also indicate the participation of lattice ^{18}O in the oxidation of CO.

O_2-TPD and TPR Studies

Figure 6 shows the O_2-TPD profiles of $YBa_2Cu_3O_{7-0.28}$ and $YBa_2Cu_3O_{7-\delta}X_\sigma$. There were two desorption peaks in each profile. For the undoped catalyst (Fig. 6(I)), the peaks appeared at ca. 570 and 720°C, corresponding to 101.6 and 32.8 μmol g^{-1} of O_2 desorption, respectively. For the five F-doped catalysts (Figs. 6(IIa–e)), with the increase in the amount of incorporated F^- ions, the temperature of the second peak shifted to lower temperature; the intensity of the first peak diminished (or even disappeared for $YBa_2Cu_3O_{7-0.18}F_{0.19}$ and $YBa_2Cu_3O_{7-0.18}F_{0.22}$), whereas that of the second peak increased. For the Cl-doped catalyst (Fig. 6(III)), the peaks were at ca. 551 and 678°C, corresponding to 18.8 and 90.6 μmol g^{-1} of O_2 desorption, respectively.

Figure 7 shows the TPR profiles of $YBa_2Cu_3O_{7-0.28}$ and $YBa_2Cu_3O_{7-\delta}X_\sigma$. One can observe that there were two reduction bands in each profile. For $YBa_2Cu_3O_{7-0.28}$, there were reductions at ca. 548 and 714°C (Fig. 7(I)). For $YBa_2Cu_3O_{7-\delta}F_\sigma$, with the rise in F content, the intensity of the first band decreased and gradually disappeared for the samples at $\sigma \geq 0.19$, whereas that of the second

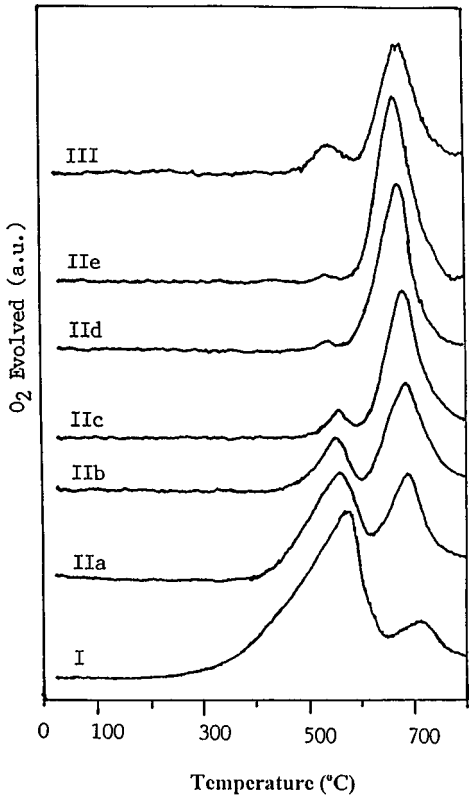

FIG. 6. O_2-TPD profiles of (I) $YBa_2Cu_3O_{7-0.28}$, (IIa–e) $YBa_2Cu_3O_{7-\delta}F_\sigma$ (same as IIa–e of Fig. 1), and (III) $YBa_2Cu_3O_{7-0.18}Cl_{0.13}$.

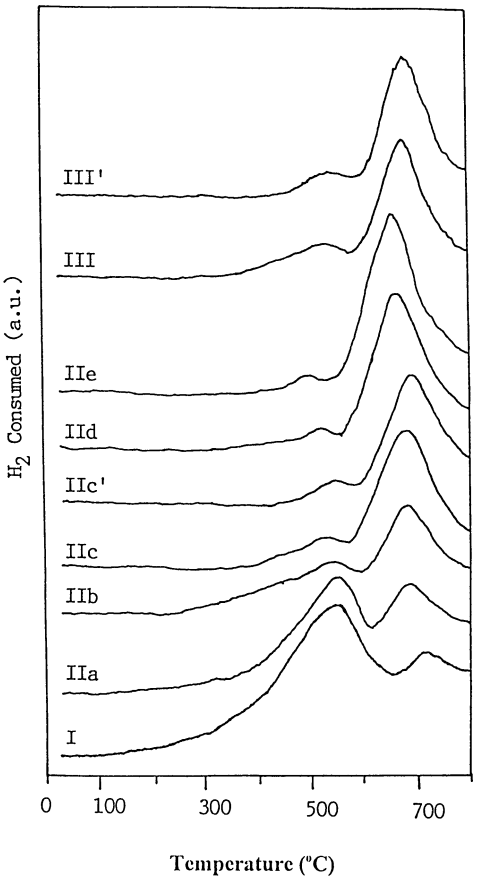

FIG. 7. TPR profiles of (I) fresh $YBa_2Cu_3O_{7-0.28}$, (IIa–e) fresh and (IIc′) used (40 h of ODE reaction) $YBa_2Cu_3O_{7-\delta}F_\sigma$ (corresponding σ values are 0.10, 0.13, 0.16, 0.19, and 0.22), and (III) fresh and (III′) used $YBa_2Cu_3O_{7-0.18}Cl_{0.13}$.

band increased; the reduction temperature of the first band altered only slightly while that of the second band shifted toward lower temperature (Figs. 7(IIa–e)). As for the $YBa_2Cu_3O_{7-0.18}Cl_{0.13}$ sample, there were two reduction bands at ca. 534 and 664°C (Fig. 7(III)); the intensities of the two bands were rather similar to those of the $YBa_2Cu_3O_{7-0.21}F_{0.16}$ catalyst. After 40 h of ODE reaction, the TPR profiles of the $YBa_2Cu_3O_{7-0.21}F_{0.16}$ and $YBa_2Cu_3O_{7-0.18}Cl_{0.13}$ samples were rather similar to the fresh samples, respectively (Figs. 7(IIc and IIc′) and 7(III and III′)). It indicates that the two catalysts were rather intact in the 40 h of on-stream testing.

DISCUSSION

Catalytic Performance

The oxidation of ethane might proceed via the following reactions:

(i) Selective oxidation:

$$C_2H_6 + (1/2)O_2 \rightarrow C_2H_4 + H_2O \quad [3]$$

(ii) incomplete oxidation:

$$C_2H_6 + (5/2)O_2 \rightarrow 2CO + 3H_2O \quad [4]$$

$$C_2H_6 + O_2 \rightarrow CO + CH_4 + H_2O \quad [5]$$

(iii) complete oxidation:

$$C_2H_6 + (7/2)O_2 \rightarrow 2CO_2 + 3H_2O \quad [6]$$

Obviously, compared to reactions [4], [5], and [6], reaction [3] consumes a smaller amount of oxygen. At a similar oxygen conversion (above 90%), C_2H_6 conversion and C_2H_4 selectivity could increase simultaneously if the incomplete and complete oxidation reactions were reduced. From Figs. 1(I–III), one can observe that with the incorporation of halide ions into the $YBa_2Cu_3O_{7-\delta}$ lattice, C_2H_6 conversion and C_2H_4 selectivity increased significantly. Usually, a comparison of C_2H_4 selectivities between various catalysts should be based on a similar level of C_2H_6 conversion. It is difficult to make such a comparison here because, at a particular C_2H_6 conversion, the reaction temperature and O_2 conversion varied significantly from catalyst to catalyst. Hence, we chose to compare the C_2H_4 selectivities and C_2H_6 conversions of the catalysts under similar reaction conditions (for example, at 680°C and at ca. 90% O_2 conversion). On the basis of similar specific surface area (Table 1) and considering the best catalysts in the superconductive perovskite series, we conclude that catalytic performance decreases in the order of $YBa_2Cu_3O_{7-0.21}F_{0.16} > YBa_2Cu_3O_{7-0.18}Cl_{0.13} \gg YBa_2Cu_3O_{7-0.28}$. Since the deep oxidation of C_2H_6 gives off much more heat than the ODE reaction, C_2H_6 conversion increased, whereas C_2H_4 selectivity decreased over $YBa_2Cu_3O_{7-0.21}F_{0.16}$ and $YBa_2Cu_3O_{7-0.18}Cl_{0.13}$ with the increase of contact time (Fig. 3). Similar results were obtained when the two catalysts were well dispersed in quartz sand (0.5 g catalyst/5.0 g quartz sand). The results illustrate that the problem of hot spots in the catalyst bed was insignificant, and the excellent performance observed is a result of real catalysis of the F- or Cl-doped perovskite materials.

For the five F-doped catalysts studied, with the increase in the amount of incorporated F^-, the nonstoichiometric oxygen, i.e., the oxygen vacancy density, decreased and the Cu^{3+} content rose. That the rise in oxygen vacancy density facilitates the total oxidation of hydrocarbons, and the rise in hypervalent *B*-site cation concentration is beneficial for the selective oxidation of hydrocarbons are known (8). The adjustment of these two opposite effects would generate a perovskite material with the amounts of oxygen vacancy and hypervalent *B*-site cation regulated for optimal catalytic performance. From the activity data in Figs. 1(II–III) and the δ and σ values as well as the Cu^{3+} contents in Table 1, one may detect a specific bulk density of oxygen vacancies and a particular Cu^{3+} content in the best-performing catalyst in the halide-doped $YBa_2Cu_3O_{7-\delta}X_\sigma$ materials. We

suggest that with the incorporation of F^- or Cl^- ions into the lattice, there is a decrease in the bulk density of oxygen vacancies and as a result, the complete oxidation reactions are reduced.

As depicted in Table 1, the undoped and halide-doped catalysts are orthorhombic. The inclusion of F^- or Cl^- ions in $YBa_2Cu_3O_{7-\delta}$ did not induce any obvious variation in crystal structure. In other words, the $YBa_2Cu_3O_{7-\delta}X_\sigma$ catalysts retained a triple-layer oxygen-deficient perovskite structure. The existence of a single-phase orthorhombic layered perovskite $YBa_2Cu_3O_{7-0.21}F_{0.16}$ or $YBa_2Cu_3O_{7-0.18}Cl_{0.13}$ means that the two substances are thermally stable at the adopted reaction temperatures (i.e., below 710°C). Furthermore, there were no significant differences in XRD patterns between the fresh and used (after 40 h of ODE reaction) samples (not shown). The halogen contents of the fresh and used catalysts were rather similar (Table 1). From the lifetime studies (Figs. 2a and 2b), one can realize that the halo-oxide catalysts were stable within a period of 40 h. These results suggested that both $YBa_2Cu_3O_{7-0.21}F_{0.16}$ and $YBa_2Cu_3O_{7-0.18}Cl_{0.13}$ are good and durable catalysts for the ODE reaction.

Defective Structure and Halogen Content

In the lattice of orthorhombic $YBa_2Cu_3O_{7-\delta}$ (Fig. 8(II)), the Ba^{2+} ions are tenfold coordinated by O^{2-} ions that form a cuboctahedron with two vertices missing. The Y^{3+} ion is eightfold coordinated by an approximate cube of O^{2-} ions. The bond distances and angles for these polyhedra are typical of the species concerned. The copper ions sit in two crystallographically distinct and chemically dissimilar sites. The Cu(1) site at (0, 0, 0) is surrounded by a square planar oxygen configuration; the Cu(2) site at (0, 0, ca. 0.3555) is fivefold coordinated by a square pyramidal arrangement of oxygens. The superconductivity in $YBa_2Cu_3O_{7-\delta}$ is very sensitive to oxygen stoichiometry (28–32). The unique role played by oxygen has motivated the investigations into the real structure of the anion sublattice of the high-temperature superconductivity (HTSC) material. Compared with the ideal perovskite structure (Fig. 8(I)), there are two principle sets of oxygen vacancies in $YBa_2Cu_3O_{7-\delta}$ (Fig. 8(II)): one layer of O^{2-} ions in the (a, b) plane surrounding the Y^{3+} ion and one line of O^{2-} ions parallel to the b-axis. The oxygen vacancy density of $YBa_2Cu_3O_{7-\delta}$ depends mainly upon the conditions adopted for preparation. David *et al.* pointed out that the site of O(3) at (1/2, 0, 0.3788) was not fully occupied (92.5 ± 3.5% occupancy) (12). Garbauskas *et al.* reported that the occupancy of oxygen site O(4) was only 72% in $YBa_2Cu_3O_{7-0.3}$ and those of O(4) and O(3) sites were, respectively, 92 and 95% in $YBa_2Cu_3O_{7-0.19}$ (33). With the rise in temperature, the oxygen atoms removed from the structure are exclusively those located at the O(4) sites (34–36); further

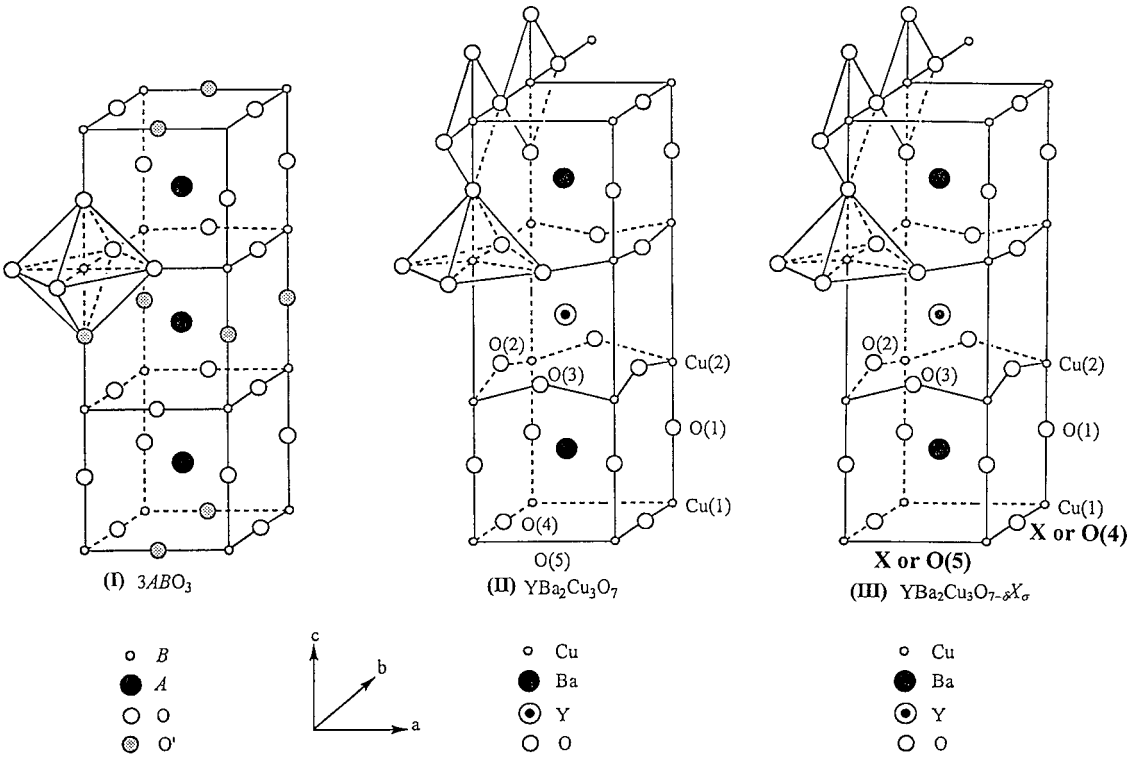

FIG. 8. Schematic structures of (I) perovskite ABO_3, (II) $YBa_2Cu_3O_7$, and (III) $YBa_2Cu_3O_{7-\delta}X_\sigma$ (X = F and Cl). The atoms O′ are the oxygen atoms of perovskite that do not exist in the structure of $YBa_2Cu_3O_7$. As a consequence of such an elimination, typical chains are formed on the basal plane of the superconductor, and the atoms Cu(2) assume fivefold pyramidal coordination.

heating at higher temperatures induces more loss of oxygen from the O(4) as well as the O(5) sites at (1/2, 0, 0) until the composition reaches a δ value of 1.0; at this stage, a structural transformation from orthorhombic to tetragonal is expected (35, 36). The δ value of the oxygen stoichiometry at such a transformation is always around 6.5. In other words, the orthorhombic phase exists over the range of $0 < \delta \leq 0.5$ and the tetragonal phase over the range of $0.5 \leq \delta < 1.0$.

Most authors believe that there are trivalent copper atoms in the superconducting material $YBa_2Cu_3O_{7-\delta}$ and these trivalent copper atoms can be distinguished from the divalent copper atoms by high-energy spectroscopic techniques such as XPS, XAS, XANES, and XES (37–40). The Cu^{3+} ions preferentially occupy the square planar Cu(1) site, a typical feature of d^8 ions (12). Actually, locating Cu^{2+} and Cu^{3+} ions on the square pyramidal Cu(2) and square planar Cu(1) sites, respectively, yields the stoichiometry $YBa_2Cu_3O_{7-\delta}$ (12). The shake-up satellites observed in the Cu $2p_{3/2}$ spectra (Fig. 4) were caused by charge transfer from neighboring oxygen ligands into an empty *d*-state of Cu^{2+} ion (41). It is expected that the satellite peak due to Cu^{2+} ion is the most predominant near the phase transition temperature where the formal oxidation state of copper is +2 and the nonstoichiometric oxygen δ is 0.5. When $\delta < 0.5$, there are Cu^{2+} and Cu^{3+} ions in $YBa_2Cu_3O_{7-\delta}$ and $YBa_2Cu_3O_{7-\delta}X_\sigma$. Since the binding energy of the 2*p* electron of Cu^{3+} ion is theoretically larger than that of Cu^{2+} ion (ca. 933.8 eV) or Cu^{2+} ion (ca. 932.7 eV) (42), another peak corresponding to Cu^{3+} ion should appear. However, we did not observe a well-resolved peak possibly due to Cu^{3+} in the XPS spectra. It is possible that the several physical processes involved in Cu photoionization have caused the broadening of the peak on the high energy side. As pointed out by Ihara *et al.* (43), the main peak of Cu 2*p* for the orthorhombic $YBa_2Cu_3O_{7-\delta}$ compound could be divided into three contributions attributable to Cu^+, Cu^{2+}, and Cu^{3+} ions, respectively. It is well known that ligand atoms can exert influence on the binding energy of metal ions (44). In $YBa_2Cu_3O_{7-\delta}X_\sigma$, the ligand atoms of copper are different from those in $YBa_2Cu_3O_{7-\delta}$. The incorporation of F or Cl atoms into the $YBa_2Cu_3O_{7-\delta}$ lattice caused the Cu $2p_{3/2}$ peak to shift to higher binding energy (Fig. 4).

For the $YBa_2Cu_3O_{7-\delta}X_\sigma$ catalysts, the halide ions replaced some of the O^{2-} ions or occupy a number of oxygen vacancies. If a F^- or Cl^- ion replaces an O^{2-} ion, in order to maintain electroneutrality, the oxidation state of an adjacent copper cation has to drop from Cu^{3+} to Cu^{2+}; if a halide ion occupies an oxygen vacancy, it would cause the oxidation state of an adjacent copper cation to rise from Cu^{2+} to Cu^{3+}. From Table 1, one may observe that the introduction of F^- or Cl^- ions into $YBa_2Cu_3O_{7-\delta}$ caused the Cu^{3+} contents to increase rather than to decrease. It demonstrates that the halide ions have occupied a certain amount of oxygen vacancies. Since oxygen sites O(4), O(5), and O(3) are not fully occupied (12), F^- or Cl^- ions could enter these oxygen sites. The pioneering work of Ovshinsky *et al.* (17) has given impetus to the investigation of the consequences of anion isomorphism in HTSCs. Adopting different preparation and characterization methods, many researchers believed the plausibility of the partial substitution of oxygen in $YBa_2Cu_3O_{7-\delta}$ by halogen atoms (45–53). It is important to confirm the presence and location of halogen atoms in the crystal lattice. All the results of a neutron-diffraction pattern analysis of fluorinated $YBa_2Cu_3O_{7-\delta}$ by LaGraff *et al.* (45) and Perrin *et al.* (46) and the anomalous scattering and EXAFS studies by Nemudry *et al.* (47) as well as the angular scanning topography and precision diffractometry studies by Ossipyan *et al.* (48) manifest that the incorporated halogen atoms occupy the vacant oxygen positions in the Cu(1) plane. Taking into consideration that the Cu^{3+} ion is located in the position of Cu(1) site (12), we propose that the halide ions should dwell in the sites of O(4) and O(5) (Fig. 8(III)). When the amount of F^- ions introduced is in excess of the amount of oxygen vacancies available, some of the F^- ions replace a certain amount of O^{2-} ions, leading to a decrease in the oxidation state of copper. Therefore, it is understandable that with the rise in F content, the Cu^{3+} content increased slightly. Taking into account the fact that the O^{2-} (radius, 1.40 Å (54)) and F^- (radius, 1.38 Å (54)) ions are similar in size whereas the Cl^- (radius, 1.81 Å (54)) ions are larger than the O^{2-} ions, the F^- ions would enter into the $YBa_2Cu_3O_{7-\delta}$ lattice more readily than the Cl^- ions and the embedding of Cl^- ions might induce the enlargement of the $YBa_2Cu_3O_{7-\delta}$ lattice.

From the O 1*s* XPS spectra, one can observe that the O 1*s* binding energy (529–530 eV) of the lattice oxygen in $YBa_2Cu_3O_{7-0.21}F_{0.16}$ and $YBa_2Cu_3O_{7-0.18}Cl_{0.13}$ was 0.7–1.0 eV higher than that (528.4 eV) in $YBa_2Cu_3O_{7-0.28}$ (Fig. 5). Due to the electronegativity of F (3.98) and Cl (3.16) (55), the inclusion of F or Cl in $YBa_2Cu_3O_{7-\delta}$ would cause the valence electron density of O^{2-} to decrease and the O 1*s* binding energy of O^{2-} to rise (Fig. 5). It means that the presence of F or Cl in the triple-layer perovskite lattice would weaken the copper–oxygen bonds. Since Cl^- ions are larger than the O^{2-} ions in size, fixing Cl^- ions in $YBa_2Cu_3O_{7-\delta}$ would cause the crystal lattice to enlarge. Based on the XRD results, the orthorhombic lattice parameters, *a*, *b*, and *c*, were estimated to be, respectively, 3.8188, 3.8836, and 11.6754 Å for $YBa_2Cu_2O_{7-0.28}$ and 3.8326, 3.8967, and 11.6764 Å for $YBa_2Cu_2O_{7-0.18}Cl_{0.13}$. That means the introduction of Cl^- ions would weaken the coulombic force between a copper cation and an O^{2-} anion. As a result, lattice O^{2-} would become more active. In other words, the inclusion of F^- or Cl^- ions in $YBa_2Cu_3O_{7-\delta}$ enhances the activity of the lattice oxygen. The increase in C_2H_4 selectivity over the halide-doped $YBa_2Cu_3O_{7-\delta}X_\sigma$ catalysts (Figs. 1(II–III)) is supporting evidence for this viewpoint.

From Table 1 and Fig. 1, one can see that among the five F-doped catalysts, with the increase in F content, the

amounts of nonstoichiometric oxygen and C_2H_6 conversion decreased whereas the Cu^{3+} content and C_2H_4 selectivity increased. When the nonstoichiometric oxygen reached 0.05, the F-containing catalyst showed the best catalytic performance. It indicates that a suitable oxygen nonstoichiometry is necessary for good activity. On the other hand, as stated above, the incorporation of F (a strong oxidizing agent) in $YBa_2Cu_3O_{7-\delta}$ induced the rise in Cu^{3+} content and enhanced the activity of lattice oxygen which is responsible for the selective oxidation of C_2H_6 to C_2H_4; the redox ability of the catalyst was strengthened as a result. Hence, the presence of more F in the lattice is beneficial to the enhancement of C_2H_4 selectivity. However, an excessive amount of F in the lattice inevitably caused the oxygen nonstoichiometry to decrease or even the destruction of the crystalline structure of Y–Ba–Cu–O ceramics due to its partial decomposition (56), and the result was a reduction in C_2H_6 conversion. Therefore, a suitable fluorine content is also needed. A proper balance of the two opposite effects would result in a catalyst of good performance. Apparently, in this study, the values of 0.05 for oxygen nonstoichiometry and ca. 27% for Cu^{3+} content in $YBa_2Cu_3O_{7-\delta}X_\sigma$ are most suitable for the ODE reaction.

Active Oxygen Species

The nature of oxygen adspecies and their relative concentrations on a catalyst surface have direct influence on the catalytic performance. Most researchers believe that among various oxygen species on/in perovskite-type oxide catalysts, O^- is accountable for the total oxidation and lattice O^{2-} close to the surface is responsible for the selective oxidation of hydrocarbons (57–59). In the ODE and OCM reactions, however, $O_2^{\delta-}$ $(0<\delta<1)$, O_2^-, O_2^{n-} $(1<n<2)$, and O_2^{2-} species are claimed to participate in the selective oxidation of ethane to ethene (60–66), whereas O^- species are prone to induce ethane deep oxidation (67). Kaliaguine *et al.* (68) analyzed the products formed in exposing the UV-irradiated V_2O_5/SiO_2 or TiO_2 catalyst to C_2H_6, and found that no C_2H_4 was generated in the reaction of O^- species with C_2H_6. Aika and Lunsford (69) proposed that O^- species on MgO abstracted a hydrogen atom from C_2H_6 to form an ethyl radical, which then reacted with O^{2-} species on MgO to give surface ethoxide ($C_2H_5O^-$) or lost another hydrogen atom to generate a small amount of C_2H_4 at 25°C. Subsequent decomposition of ethoxide above 300°C produced a larger amount of C_2H_4. Based on the investigation on various oxygen species formed on MgO-based catalysts (69–73), Lunsford *et al.* concluded that the reactivity of these oxygen species toward hydrocarbons follows the order of $O^- \gg O_3^- \gg O_2^{2-} > O_2^- > O^{2-}$. It is generally accepted that in the conversion of hydrocarbons, O^- species foment total oxidation, whereas O^{2-} species induce selective oxidation (57–59, 74).

The α and β desorption peaks in O_2-TPD chromatograms are known characteristics of most perovskites. The former is due to oxygen accommodated in oxygen vacancies (8, 75); this type of dissociatively adsorbed species is believed to be responsible for the complete oxidation of hydrocarbons (57, 58). As for β desorption, the oxygen can be associated with the partial reduction of *B*-site cations by lattice oxygen (8), and such oxygen is reckoned to be responsible for the selective oxidation of hydrocarbons (57, 58). The complete substitution of Sr for La in $La_{1-x}Sr_xFeO_{3-\delta}$ leads to the increase in oxygen vacancies; consequently, the amount of α oxygen is increased and the ability for complete oxidation strengthened. However, with the introduction of halide ions into the $SrFeO_{3-\delta}$ lattice, the drop in oxygen vacancy density (due to occupation by the halide ions) means a decrease in α oxygen density and a rise in selective oxidation ability (19). In the $YBa_2Cu_3O_{7-\delta}$ and $YBa_2Cu_3O_{7-\delta}X_\sigma$ catalysts, O^- species adsorbed at oxygen vacancies abstracted a hydrogen atom from C_2H_6 to form a C_2H_5 radical and then a lattice O^{2-} reacted with the C_2H_5 radical to generate a $C_2H_5O^-$ species which decomposes to give C_2H_4. It is clear that an excessive amount of O^- species would lead to C_2H_6 and C_2H_4 deep oxidation, and too low an activity of lattice oxygen would hinder the formation of $C_2H_5O^-$; both are factors unfavorable for the ODE reaction. With a suitable amount of oxygen vacancies and enhanced lattice oxygen activity, $YBa_2Cu_3O_{7-0.21}F_{0.16}$ and $YBa_2Cu_3O_{7-0.18}Cl_{0.13}$ showed the best catalytic performance.

By determining the exact oxygen composition of $La_{1-x}Sr_xCoO_{3-\delta}$ $(x=0$–$1)$ before and after the respective desorption peaks, Yamazoe *et al.* pointed out that a certain amount of Co^{4+} ion was actually induced by the oxygen dissociatively adsorbed at oxygen vacancies (76). Generally speaking, only after calcination in an O_2-containing atmosphere would the oxygen vacancies in a catalyst be occupied by dissociatively adsorbed oxygen (O^-). In the calcined $YBa_2Cu_3O_{7-\delta}X_\sigma$ catalysts, some Cu^{3+} ions were formed due to the occupancy of oxygen vacancies by O^-. The detection of the signal at ca. 531 eV O 1*s* binding energy (Figs. 5(I–III)) indicated the presence of O^- species in these catalysts. These results demonstrate that there were O^- species accommodated in the oxygen vacancies, driving the Cu^{3+} content to rise. As halide leaching was insignificant (Tables 1 and 4), we consider that the weight losses observed in the TGA studies were due to the desorption of oxygen species via two steps:

$$\text{StepI}: \ YBa_2Cu_3O_{7-\delta}X_\sigma \xrightarrow{\alpha\ \text{oxygen}} YBa_2Cu_3O_{7-\delta 1}X_{\sigma 1} \quad (\delta 1=\delta, \sigma 1=\sigma)$$

$$\text{StepII}: \ YBa_2Cu_3O_{7-\delta 1}X_{\sigma 1} \xrightarrow{\beta\ \text{oxygen}} YBa_2Cu_3O_{7-\delta 2}X_{\sigma 2} \quad (\delta 2=\delta 1+(3Cu^{3+}-\sigma)/2, \sigma 2=\sigma).$$

From Table 3, one may ascribe the weight losses below

TABLE 6

The Compositions of $YBa_2Cu_3O_{7-0.28}$, $YBa_2Cu_3O_{7-0.21}F_{0.16}$, and $YBa_2Cu_3O_{7-0.18}Cl_{0.13}$ after Step I at 610°C and Step II at 710°C

	Step I (at 610°C)				Step II (at 710°C)			
Catalyst	Cu^{3+} Content (mol%)	$\delta 1$	$\sigma 1$	O_2 Evolved (wt%)	Cu^{3+} Content (mol%)	$\delta 2$	$\sigma 2$	O_2 Evolved (wt%)
$YBa_2Cu_3O_{7-0.28}$	14.9	0.28	—	0.65	9.6	0.36	—	0.19
	(14.7)[a]	(0.28)	(—)	(0.66)	(9.2)	(0.36)	(—)	(0.20)
$YBa_2Cu_3O_{7-0.21}F_{0.16}$	25.0	0.20	0.16	0.10	9.5	0.44	0.16	0.56
	(24.9)	(0.21)	(0.16)	(0.11)	(9.1)	(0.44)	(0.16)	(0.57)
$YBa_2Cu_3O_{7-0.18}Cl_{0.13}$	25.7	0.18	0.13	0.11	10.9	0.40	0.13	0.53
	(25.8)	(0.18)	(0.13)	(0.10)	(10.1)	(0.41)	(0.13)	(0.56)

Note. Also listed are the O_2 evolved in both steps.

[a] Values in parentheses were estimated according to the data obtained in thermal treatments.

610°C over these catalysts to the desorption of α oxygen (8) via Step I and those between 610 and 800°C to the desorption of lattice (β) oxygen (77) via Step II. For all the catalysts, the weight losses were rather close to those due to the desorption of O^- located in oxygen vacancies (all the oxygen vacancies were presumably occupied by O^-) below 610°C, whereas between 610 and 800°C, the weight loss values were less than those estimated based on partial Cu^{3+} reduction. Among the F-doped catalysts, with the increase in fluoride ion content, the amounts of desorbed α oxygen decreased, whereas those of β oxygen increased. It indicates that the addition of fluoride ions enhanced the activity of lattice O^{2-}. It can be observed that the $YBa_2Cu_3O_{7-0.21}F_{0.16}$ and $YBa_2Cu_3O_{7-0.18}Cl_{0.13}$ catalysts that performed the best had similar weight losses in the two temperature ranges. Obviously, the weight losses in the halo-oxide catalysts were quite close to the estimated values, whereas for the undoped catalyst, although the weight loss of 0.74 wt% below 610°C agreed with the predicted value of α oxygen, the weight loss of 0.19 wt% between 610 and 800°C was much less than the predicted figure (0.54 wt%) of β oxygen, indicating that the lattice O^{2-} in $YBa_2Cu_3O_{7-0.28}$ was much less active than those in $YBa_2Cu_3O_{7-0.21}F_{0.16}$ and $YBa_2Cu_3O_{7-0.18}Cl_{0.13}$. From Table 4, one can observe that in a He atmosphere, most of the O^- species in $YBa_2Cu_3O_{7-0.28}$ desorbed at 610°C, resulting in a weight loss of 0.66 wt%, a value rather close to the theoretical value (0.68 wt%) of Step I; and there was a noticeable decrease in Cu^{3+} content. Between 610 and 710°C, the Cu^{3+} content decreased by ca. 37% and the weight loss was 0.20 wt%. The results indicate that a large extent of weight loss was due to the desorption of α oxygen and the lattice O^{2-} was not active in $YBa_2Cu_3O_{7-0.28}$. As for $YBa_2Cu_3O_{7-0.21}F_{0.16}$ and $YBa_2Cu_3O_{7-0.18}Cl_{0.13}$, however, with the rise in treatment temperature, the decreases in Cu^{3+} content were significant and the weight losses of 0.57 and 0.56 wt% were getting close to the expected values (0.70 and 0.77 wt%) of Step II, respectively. These results indicate that the introduction of F^- or Cl^- ions into $YBa_2Cu_3O_{7-\delta}$ enhanced the activity of lattice O^{2-}. Passing oxygen through the catalysts that had just been thermally treated in He would restore the Cu^{3+} contents to the former values (Table 1). The results demonstrate that the oxygen consumed in the ODE reaction could be replenished by the oxygen from the gas phase according to the sequence

$$O_2(g) \rightarrow O_2^-(ads) \rightarrow O_2^{2-}(ads) \rightarrow 2O^-(ads) \rightarrow 2O^{2-}(ads) \rightarrow 2O^{2-}_{lattice}. \quad [7]$$

From Table 6, one can realize that the Cu^{3+} content, $\delta 1$ (or $\delta 2$), $\sigma 1$ (or $\sigma 2$), and the amounts of evolved O_2, via either Step I or Step II, were quite close to those estimated according to the data obtained in thermal treatments. When the treatment temperature was raised from 610 to 710°C, with the removal of lattice O^{2-} from the three catalysts due to the partial reduction of Cu^{3+} ions, the oxygen vacancy density increased. When a C_2H_6 pulse was introduced, respectively, to the three catalysts at 500°C, $YBa_2Cu_3O_{7-0.28}$ showed the highest C_2H_6 conversion but poorest C_2H_4 selectivity, confirming that α oxygen is responsible for the complete oxidation of C_2H_6 and C_2H_4. At 610 or 710°C, C_2H_6 conversion and C_2H_4 selectivity recorded either in a pulse of C_2H_6 or in a pulse of C_2H_6/O_2 increased significantly over the three catalysts, indicating that β oxygen (i.e., lattice oxygen) is accountable for the selective oxidation of C_2H_6 to C_2H_4. The direct evidence for the involvement of $YBa_2Cu_3O_{7-\delta}X_\sigma$ lattice oxygen in the reaction with C_2H_6 or CO is from the isotope $^{18}O_2$-pulsing experiments. During the study of ^{18}O–^{16}O substitution on $YBa_2Cu_3O_{7-\delta}$ via gas-exchange, Franck *et al.* found that the O(4), O(5), O(3), and O(2) oxygens are relatively more prone to substitution (78). After thermal desorption of O_2 in He at 710°C, the ^{18}O introduced into the system entered into the positions [O(4), O(5), O(3), and/or O(2) sites] previously occupied by lattice oxygen via sequence [7] at 610°C. The lattice ^{18}O reacted with C_2H_6 or CO to generate $H_2{}^{18}O$ or $CO{}^{18}O$. These

results indicate that the oxygen species evolved at 610–710°C are indeed lattice oxygen in the $YBa_2Cu_3O_{7-\delta}X_\sigma$ catalysts. It also implies that via step [7], gaseous O_2 molecules could replenish a catalyst with lattice oxygen.

The inclusion of F^- or Cl^- ions in $YBa_2Cu_3O_{7-0.28}$ gives rise to two effects: (i) the decrease in the amount of oxygen vacancy, i.e., the decrease in α oxygen concentration; (ii) the rise in Cu^{3+} content, i.e., the promotion of β oxygen desorption. As shown in the O_2-TPD studies, with the addition of F^- or Cl^- ions to $YBa_2Cu_3O_{7-0.28}$, the α oxygen peak at ca 500°C decreased, whereas the β oxygen peak increased in intensity (Figs. 6(IIa–e) and 6(III)). It is clear that the concentration and distribution of oxygen species on/in $YBa_2Cu_3O_{7-0.21}F_{0.16}$ and $YBa_2Cu_3O_{7-0.18}Cl_{0.13}$ were different from those on/in $YBa_2Cu_3O_{7-0.28}$. As shown in Fig. 2, the $YBa_2Cu_3O_{7-0.21}F_{0.16}$ and $YBa_2Cu_3O_{7-0.18}Cl_{0.13}$ catalysts showed high C_2H_4 selectivities at the temperatures ranging from 600 to 680°C, coinciding the temperatures for β oxygen desorptions (Figs. 6(IIa–e) and 6(III)). Therefore, we suggest that the oxygen species that desorbed within the 610–710°C range are the active species for the selective oxidation of ethane.

For the undoped $YBa_2Cu_3O_{7-0.28}$ catalyst, there were two reduction bands: the band at ca. 548°C was much larger in intensity than the band at ca. 714°C (Fig. 7(I)). For the halide-doped $YBa_2Cu_3O_{7-\delta}X_\sigma$ catalysts, there were two bands in the TPR profiles, one in the 530–540°C range and the other in the 660–680°C range (Figs. 7(IIa–e) and 7(III)). Compared to the O_2-TPD results, we know that the TPR band in the 530–540°C range and the band in the 660–680°C range are due to the reduction of α and β oxygen species, respectively. These results indicate that after the incorporation of the halide ions into the perovskite lattice, the amount of α oxygen diminished to extinction while the amount of β oxygen increased. According to the nature of α and β oxygens, one can deduce that the oxygen vacancy density decreased while the Cu^{3+} content rose in the $YBa_2Cu_3O_{7-\delta}X_\sigma$ materials. This is in good agreement with the data in Table 1. The reduction temperatures (Figs. 7(IIa–e) and 7(III)) also coincide with the temperatures at which the catalysts performed well (Fig. 1). The TPR profiles of the fresh and the used samples (Figs. 7(IIc and IIc′) and 7(III and III′)) are rather similar, indicative of good stability of the perovskite-type halo-oxide catalysts.

CONCLUSIONS

The incorporation of F^- or Cl^- ions in the $YBa_2Cu_3O_{7-\delta}$ lattice could significantly enhance the catalytic performance for the selective oxidation of C_2H_6 to C_2H_4. We found that orthorhombic triple-layered perovskite-type $YBa_2Cu_3O_{7-0.21}F_{0.16}$ and $YBa_2Cu_3O_{7-0.18}Cl_{0.13}$ performed the best among the halide-doped $YBa_2Cu_3O_{7-\delta}$ catalysts. The inclusion of F^- or Cl^- ions in $YBa_2Cu_3O_{7-\delta}$ enhanced the activity of lattice oxygen. A suitable combination of oxygen nonstoichiometry and Cu^{3+} concentration in $YBa_2Cu_3O_{7-\delta}X_\sigma$ is required for the best catalytic performance of the catalysts. It is suggested that the O^- species adsorbed at oxygen vacancies are responsible for C_2H_6 deep oxidation whereas surface and subsurface lattice oxygen species are active for C_2H_6 selective oxidation to C_2H_4.

ACKNOWLEDGMENTS

The work described above was fully supported by a grant from the Research Grants Council of the Hong Kong Special Administration Region, P. R. China (Project No. HKBU 2015/99P). H. X. Dai thanks the HKBU for a Ph.D. studentship.

REFERENCES

1. Wang, D., Rosynek, M. P., and Lunsford, J. H., *J. Catal.* **151**, 155 (1995).
2. Ueda, W., Lin, S. W., and Tohmoto, I., *Catal. Lett.* **44**, 241 (1996).
3. Omata, K., Yamazaki, O., Tomita, K., and Fujimoto, K., *J. Chem. Soc. Chem. Commun.* 1647 (1994).
4. Lin, Y. S., and Zeng, Y., *J. Catal.* **164**, 220 (1996).
5. Nozaki, T., and Fujimoto, K., *AIChE J.* **40**, 870 (1994).
6. ten Helshof, J. E., Bouwmeester, H. J. M., and Verweeij, H., *Appl. Catal. A* **130**, 195 (1995).
7. Yi, G. H., Hayakawa, T., Anderson, A. G., Suzuki, K., Hamakawa, S., York, A. P. E., Shimizu, M., and Takehira, K., *Catal. Lett.* **38**, 189 (1996).
8. Seiyama, T., in "Properties and Application of Perovskite-Type Oxides" (L. G. Tejuca and J. L. G. Fierro, Eds.). Marcel Dekker, New York, 1993.
9. Viswanathan, B., in "Properties and Application of Perovskite-Type Oxides" (L. G. Tejuca and J. L. G. Fierro, Eds.). Marcel Dekker, New York, 1993.
10. Wu, M. K., Ashburn, J. R., Torng, C. J., Hor, P. H., Meng, R. L., Gao, L., Huang, Z. J., Wang, Y. Q., and Chu, C. W., *Phys. Rev. Lett.* **58**, 908 (1987).
11. Cava, R. T., Baltogg, B., Chen, C. H., Rietman, E. A., Zahurak, S. M., and Werder, D., *Nature* **329**, 423 (1987).
12. David, W. I. F., Harrison, W. T. A., Gunn, J. M. F., Moze, O., Soper, A. K., Day, P., Jorgensen, J. D., Hinks, D. G., Beno, M. A., Soderholm, L., Capone II, D. W., Schuller, I. K., Segre, C. U., Zhang, K., and Grace, J. D., *Nature* **327**, 310 (1987).
13. Cox, D. E., Moodenbaugh, A. R., Hurst, J. J., and Jones, R. H., *J. Phys. Chem. Solids* **49**, 47 (1987).
14. Hansen, S., Otamiri, J., Bovin, J. O., and Andersson, A., *Nature* **334**, 143 (1988).
15. Mizuno, N., Yamato, M., and Misono, M., *J. Chem. Soc. Chem. Commun.* 887 (1988).
16. Jiang, A. R., Peng, Y., Zhou, Q. W., Gao, P. Y., Yuan, H. Q., and Deng, J. F., *Catal. Lett.* **3**, 235 (1989).
17. Ovshinsky, S. R., Young, R. T., Allred, D. D., Demaggio, G., and van der Leeden, G. A., *Phys. Rev. Lett.* **58**, 2579 (1987).
18. Lee, I., and Ng, K. Y. S., *Catal. Lett.* **2**, 403 (1989).
19. Dai, H. X., Ng, C. F., and Au, C. T., *Catal. Lett.* **57**, 115 (1999).
20. Dai, H. X., Ng, C. F., and Au, C. T., *J. Catal.* **189**, 52 (2000).
21. Bhalla, A. S., Rustum, R., and Cross, L. E., in "Chemistry of Oxide Superconductivity" (C. N. R. Rao, Ed.). Blackwell, Oxford, 1988.
22. Au, C. T., Liu, Y. W., and Ng, C. F., *J. Catal.* **176**, 365 (1998).
23. Oku, M., Kimura, J., Hosoya, M., Takada, K., and Hirokawa, K., *Fresenius Z. Anal. Chem.* **332**, 237 (1988).
24. Saito, Y., Noji, T., Hirokawa, K., Endo, A., Matsuzaki, N., Katsumata, M., and Higuchi, N., *Jpn. J. Appl. Phys.* **26**, L838 (1987).

25. Shafer, M. W., Penney, T., and Olson, B. L., *Phys. Rev. B* **36**, 4047 (1987).
26. Fukushima, N., Yoshino, H., Niu, H., Hayashi, M., Saaski, H., Yamada, Y., and Murase, S., *Jpn. J. Appl. Phys.* **26**, L719 (1987).
27. Rao, C. N. R., in "Chemistry of Oxide Superconductivity" (C. N. R. Rao, Ed.). Blackwell, Oxford, 1988.
28. Rao, C. N. R., and Ganguly, P., *Jpn. J. Appl. Phys.* **26**, L882 (1987).
29. Rao, C. N. R., Ganguly, P., Gopalakrishnan, J., and Sarma, D. D., *Mat. Res. Bull.* **22**, 1159 (1987).
30. Johnston, D. C., Jacoson, A. J., Newsam, J. M., Lewandowski, J. T., Goshorn, D. P., Xie, D., and Yelon, W. B., *ACS Symposium Series* 351, 1987.
31. Murphy, D. W., Sunshine, S. A., Gallagher, P. K., O'Bryan, H. M., Cava, R. J., Batlogg, B., van Dover, R. B., Scheemeyer, L. F., and Zahurak, S. M., *ACS Symposium Series* 351, 1987.
32. Tarascon, J. M., Barboux, P., Bagley, B. G., Greene, L. H., McKinnon, W. R., and Hull, G. W., *ACS Symposium Series* 351, 1987.
33. Garbauskas, M. F., Arendt, R. H., and Kasper, J. S., *Inorg. Chem.* **26**, 3191 (1987).
34. Beech, F., Miraglia, S., Santoro, A., and Roth, R. S., *Phys. Rev. B* **35**(16), 8778 (1987).
35. Jorgensen, J. D., Beno, M. A., Hinks, D. G., Soderholm, L., Volin, K. J., Hitterman, R. L., Grace, J. D., Schuller, I. K., Segre, C. U., Zhang, K., and Kleefisch, M. S., *Phys. Rev. B* **36**(7), 3608 (1987).
36. Grader, G. S., and Gallagher, P. K., *Adv. Cer. Mat.* **2**, 649 (1987).
37. Lytle, F. W., Greegor, R. B., and Panson, A. J., *Phys. Rev. B* **37**, 1550 (1988).
38. Balzarotti, A., De Crescenzi, M., Motta, N., Patella, F., and Sgarlata, A., *Phys. Rev. B* **38**, 6461 (1988).
39. Steiner, P., Hüfner, S., Kinsinger, V., Sander, I., Siegwart, B., Schmitt, H., Schulz, R., Junk, S., Schwitzgebel, G., Gold, A., Politis, C., Müller, H. P., Hoppe, R., Kemmler-Sack, S., and Kunz, C., *Z. Phys. B* **69**, 449 (1988).
40. Jasiolek, G., Pajaczkowska, A., and Przyslupski, P., *Z. Phys. B* **72**, 7 (1988).
41. Kim, K. S., *J. Electron. Spectrosc.* **3**, 217 (1974).
42. Shin, J. S., Enomoto, H., Takauchi, H., Takno, Y., Mori, N., and Ozaki, H., *Jpn. J. Appl. Phys.* **28**, L1365 (1989).
43. Ihara, H., Hirabayashi, M., Terada, N., Kimura, Y., Senzaki, K., Akimoto, M., Bushida, K., Kawashima, F., and Uzuka, R., *Jpn. J. Appl. Phys.* **26**, L460 (1987).
44. Healy, P. C., Myhra, S., and Stewart, A. M., *Jpn. J. Appl. Phys.* **26**, L1884 (1987).
45. LaGraff, J. R., Behrman, E. C., Taylor, J. A. T., Rotella, E. J., Jorgensen, J. D., Wang, L. Q., and Mattocks, P. G., *Phys. Rev. B* **39**, 347 (1989).
46. Perrin, C., Dinia, A., Pena, O., Sergent, M., Burlet, P., and Rossat-Mignod, J., *Solid State Commun.* **76**, 401 (1990).
47. Nemudry, A. P., Pavlyukhin, Y. T., Khainovskii, N. G., and Boldyrev, V. V., *Superconductivity* **3**, 1528 (1990). [In Russian]
48. Ossipyan, Yu. A., Zharikov, O. V., Logvenov, G. Yu., Sidorov, N. S., Kulakov, V. I., Shmytko, I. M., Bdikin, I. K., and Gromov, A. M., *Physica C* **165**, 107 (1990).
49. Klimenko, A. G., Ishikaev, S. M., Mironov, Yu. I., Fedin, V. P., Fedorov, V. E., and Sheer, M., *Superconductivity* **2**, 142 (1989). [In Russian]
50. Perrin, C., Pena, O., and Sergent, M., "Conference on High-Temperature Superconductors, Material Aspects." Deutsche Gesellschaft für Materialkunde, Oberursel, 1990.
51. Radousky, H. B., Glass, R. S., Hahn, P. A., Fluss, M. J., Meisenheimer, R. G., Nonner, B. P., Mertzbacher, C. I., Larson, E. M., Keegan, K. D., O'brien, J. C., Peng, J. L., Shelton, R. N., and McCarty, K. F., *Phys. Rev. B* **41**, 11140 (1990).
52. Perrin, C., Pena, O., Sergent, M., Christensen, P., Fonteneau, G., and Lucas, J., *Supercond. Sci. Technol.* **2**, 35 (1989).
53. Conard, J., Perrin, C., Pena, O., Sergent, M., and Fonteneau, G., *Synthetic Metals* **34**, 461 (1989).
54. Cotton, F. A., and Wilkinson, G., "Advanced Inorganic Chemistry," 3rd ed. Interscience, New York, 1972.
55. Lide, D. R. (Ed.), "Handbook of Chemistry and Physics." CRC Press, New York, 1998–1999.
56. Ossipyan, Yu. A., Zharikov, O. V., and Nikolaev, R. K., in "The Real Structure of High-T_c Superconductors" (V. Sh. Shekhtman, Ed.). Springer-Verlag, Berlin, 1993.
57. Bielañski, A., and Haber, J., "Oxygen in Catalysis." Marcel Dekker, New York, 1991.
58. Haber, J., in "Surface Properties and Catalysis by Non-Metals" (J. P. Bonnelle, B. Delmon, and E. Derouane, Eds.). Reidel, Dordrecht, 1983.
59. Tagawa, T., and Imai, H., *J. Chem. Soc., Faraday Trans. I* **84**, 923 (1988).
60. Dissanayake, D., Lunsford, J. H., and Rosynek, M. P., *J. Catal.* **143**, 286 (1993).
61. Mestl, G., Knözinger, H., and Lunsford, J. H., *Ber. Bunsenges. Phys. Chem.* **97**, 319 (1993).
62. Lunsford, J. H., Yang, X., Haller, K., Laane, J., Mestl, G., and Knözinger, H., *J. Phys. Chem.* **97**, 13810 (1993).
63. Au, C. T., Liu, Y. W., and Ng, C. F., *J. Catal.* **171**, 231 (1997).
64. Au, C. T., Zhou, X. P., Liu, Y. W., Ji, W. J., and Ng, C. F., *J. Catal.* **174**, 153 (1998).
65. Au, C. T., Chen, K. D., Dai, H. X., Liu, Y. W., Luo, J. Z., and Ng, C. F., *J. Catal.* **179**, 300 (1998).
66. Au, C. T., Chen, K. D., Dai, H. X., Liu, Y. W., and Ng, C. F., *Appl. Catal. A* **177**(2), 185 (1999).
67. Dai, H. X., Liu, Y. W., Ng, C. F., and Au, C. T., *J. Catal.* **187**, 59 (1999).
68. Kaliaguine, S. L., Shelimov, B. N., and Kazansky, V. B., *J. Catal.* **55**, 384 (1978).
69. Aika, K., and Lunsford, J. H., *J. Phys. Chem.* **81**, 1393 (1977).
70. Aika, K., and Lunsford, J. H., *J. Phys. Chem.* **82**, 1794 (1978).
71. Takita, Y., and Lunsford, J. H., *J. Phys. Chem.* **83**, 683 (1979).
72. Takita, Y., Iwamoto, M., and Lunsford, J. H., *J. Phys. Chem.* **84**, 3079 (1980).
73. Iwamoto, M., and Lunsford, J. H., *J. Phys. Chem.* **84**, 1710 (1980).
74. Libre, J. M., Parbaux, Y., Grzybowska, B., Conflant, P., and Bonnelle, J. P., *Appl. Catal.* **6**, 315 (1983).
75. Zhang, H. M., Shimizu, Y., Teraoka, Y., Miura, N., and Yamazoe, N., *J. Catal.* **121**, 432 (1990).
76. Yamazoe, N., Teraoka, Y., and Seiyama, T., *Chem. Lett.* 1767 (1981).
77. Wu, Y., Yu, T., Dou, B. S., Wang, C. X., Xie, X. F., Yu, Z. L., Fan, S. R., Fan, Z. R., and Wang, L. C., *J. Catal.* **120**, 88 (1989).
78. Franck, J. P., Jung, J., Salomons, G., Miner, W. A., Mohamed, M. A.-K., Chrzanowski, J., Gygax, S., Irwin, J. C., Mitchell, D. F., and Sproule, G. I., *Physica C* **172**, 90 (1990).